ASCE

Earthquake and Postearthquake Fire Testing of a Midrise Cold-Formed Steel-Framed Building. II: Shear Wall Behavior and Design Implications

Xiang Wang[1] and Tara C. Hutchinson, M.ASCE[2]

Abstract: Complementing a companion paper that summarizes the building global response and physical damage of a midrise cold-formed steel (CFS) framed building during an earthquake and postearthquake fire test program, this paper focuses on understanding the seismic behavior of the shear walls utilized in the building system during this test program. In contrast to shear walls tested in an isolated configuration, the shear walls within the full-scale test building were constructed and tested under real-world kinematic constraints and dynamic loading environments. The shear walls located at various planar and vertical locations of the test building were instrumented with a dense array of analog sensors to monitor the shear wall local responses. In this study, the shear wall local responses are correlated with the global responses of the building to advance understanding regarding the behavioral characteristics of individual shear walls and in particular the interactions of the shear walls as part of the lateral-load-resisting system. Important seismic design parameters are inferred from the measured building response using a parameter optimization strategy. Their implications associated with the seismic design of CFS wall-framed structural systems are discussed in relation to code provisions and design guidelines. **DOI: 10.1061/(ASCE)ST.1943-541X.0003098.**

Author keywords: Cold-formed steel (CFS); Seismic design; Shake-table testing; Steel-sheathed shear walls.

Introduction

Shear walls are common lateral-load-resisting elements utilized in light-framed cold-formed steel (CFS) construction. These structural elements must provide sufficient lateral strength and deformation capacity to ensure the life-safety performance of a building system in the event of an earthquake. Prior experimental research on component-level shear wall behavior supports seismic design guidelines of CFS wall-braced structures. However, the CFS shear wall components within a structural system observe different boundary conditions and kinematic demands than those placed in an isolated configuration. Therefore, their seismic behavior may be modified due to the interactions with other shear walls and other structural elements (e.g., gravity walls and floor diaphragms).

A large body of experimental data obtained from component-level shear wall tests has contributed to the development of seismic design guidelines for CFS shear walls with varied sheathing and framing details. Such studies involved testing of CFS shear walls sheathed with sheet steel (e.g., Yu 2010; Balh et al. 2014), oriented strand board (OSB) panels (e.g., Serrette et al. 1997; Fülöp and Dubina 2004; Liu et al. 2014), corrugated steel (e.g., Zhang et al. 2016, 2017), and strap-braced shear walls (e.g., Iuorio et al. 2014). However, very few experimental investigations have been undertaken to understand the seismic behavior of these components within a structural system under realistic dynamic loading and boundary conditions. Research of this kind has only occurred in a handful of shake-table experiments of low-rise CFS-framed buildings (e.g., Peterman et al. 2016a, b; Fiorino et al. 2017, 2019).

In light of the aforementioned paucity of experimental data regarding the seismic behavior of CFS structural systems and their structural elements in a system-level arrangement, a full-scale building test program was conducted on the Large High-Performance Outdoor Shake Table (LHPOST) at the University of California, San Diego (UCSD) (Wang et al. 2016). The test building was subjected to a sequence of earthquake and live fire tests in three separate test phases, namely prefire earthquake, postearthquake fire, and postfire earthquake phases. These system-level building tests permitted investigation of the seismic behavior of shear walls under realistic earthquake loading environments and practical boundary conditions. Complementing a companion paper (Hutchinson et al. 2021) that summarizes the building global responses and its physical damage during the multihazard test program, the present paper focuses on understanding the seismic behavior of the CFS shear walls within a system-level arrangement. Shear walls located at three select levels of the building, namely Levels 1, 2, and 4, were instrumented with a dense array of analog sensors to monitor their local seismic responses such as sheathing panel shear deformations and tie-rod forces.

In this paper, the shear wall local responses measured during the earthquake tests are investigated and correlated with the building global responses to advance understanding of the seismic behavior of the shear walls and in particular the interactions of different shear walls as part of the lateral-load-resisting system (e.g., shear walls located along the same wall line or in the same quadrant). Important CFS seismic design parameters are inferred from the measured building response using a parameter optimization strategy. Their implications associated with the seismic design of CFS wall-framed

[1]Postdoctoral Researcher, Dept. of Structural Engineering, Univ. of California, San Diego, La Jolla, CA 92093-0085 (corresponding author). ORCID: https://orcid.org/0000-0002-9845-1875. Email: xiw002@eng.ucsd.edu; xiw002@ucsd.edu

[2]Professor, Dept. of Structural Engineering, Univ. of California, San Diego, La Jolla, CA 92093-0085. ORCID: https://orcid.org/0000-0001-9109-7896

Note. This manuscript was submitted on June 18, 2020; approved on April 8, 2021; published online on June 28, 2021. Discussion period open until November 28, 2021; separate discussions must be submitted for individual papers. This paper is part of the ***Journal of Structural Engineering***, © ASCE, ISSN 0733-9445.

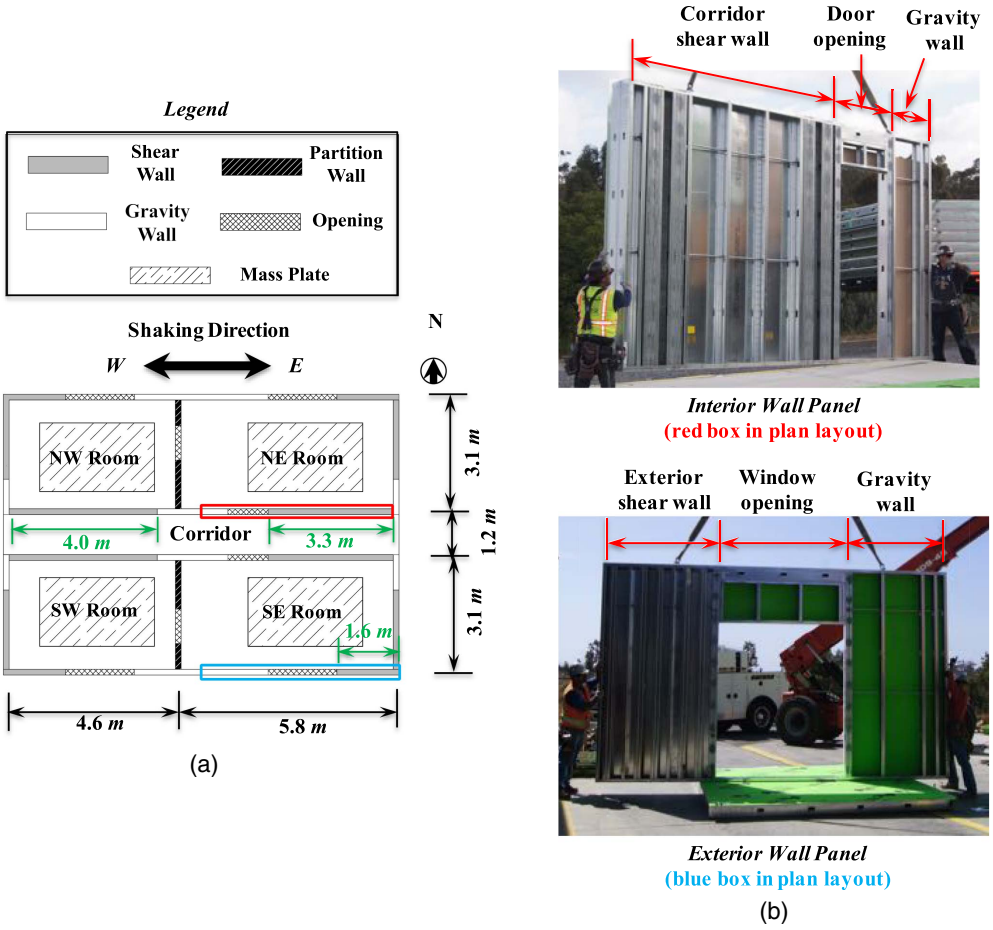

Fig. 1. (a) Test building plan layout representative of Levels 2–6 (transverse partition walls were not installed at Level 1); and (b) prefabricated wall panels (images by Xiang Wang).

structural systems are discussed in relation to code provisions and guidelines.

Steel-Sheathed Shear Walls in the Test Building

The full-scale 6-story CFS test building was designed to carry gravity and lateral seismic loading via a combination of prefabricated CFS floor diaphragms and walls sheathed with sheet steel (Fig. 1). Emulating the compartmentalized architectural layout of a multistory residential building, the plan configuration of the building was designed with four distinct rooms, a pair of each separated by a long corridor, whose length aligned with the axis of shaking direction of the shake table. As such, two longitudinal shear walls were placed along each of the east and west ends of the corridor, with an associated wall length of 4.0 m (13 ft) for the walls at the west end and 3.3 m (11 ft) at the east end. In addition, shear walls with a length of ~1.6 m (5 ft 4 in.) in the longitudinal direction and ~2.1 m (7 ft) in the transverse direction were placed on the exterior of the building at its four corners. For brevity, the longitudinal and transverse exterior walls at the corners may be collectively referred to as corner shear walls. The interior corridor shear walls were designed as the primary lateral-load-resisting elements in the direction of shaking, whereas the exterior corner shear walls were intended to resist transverse and torsional seismic loads.

To facilitate the presentation of shear wall local responses, this section summarizes the framing and sheathing details of the corridor and corner walls as well as the associated instrumentation plan, whereas further information regarding the overall test program and global building response are discussed in a companion paper (Hutchinson et al. 2021). Importantly, this midrise test building adopted a unique restraint system to resist seismic uplift forces of the building via the use of continuous steel rods and light-frame compression stud packs embedded within the two ends of individual shear walls. Because the seismic behavior of the steel tie rods of the restraint system provided essential information for investigating the interaction among the shear walls and surrounding nondesignated structural components (e.g., gravity walls), details of this restraint system are articulated in this section.

Framing and Sheathing Details

The shear walls were constructed using standard CFS framing members (e.g., top and bottom tracks and repetitively placed vertical studs) (Fig. 2). The corridor walls were fabricated using vertical studs 600S200-68 at the first level and 600S200-54 at all remaining levels, whereas the corner walls utilized vertical studs 600S200-54 at 610 mm (24 in.) on center (o.c.) at all levels. Sheathing materials utilized load-resisting structural panels on the exterior (or corridor) side and 16 mm (5/8 in.) thick regular gypsum boards on the interior (room) side. The structural panels were fabricated using 16 mm (5/8 in.) thick gypsum boards bonded with a layer of 0.686 mm (0.027 in.) thick (22 gauge) sheet steel to provide lateral resistance to the shear walls.

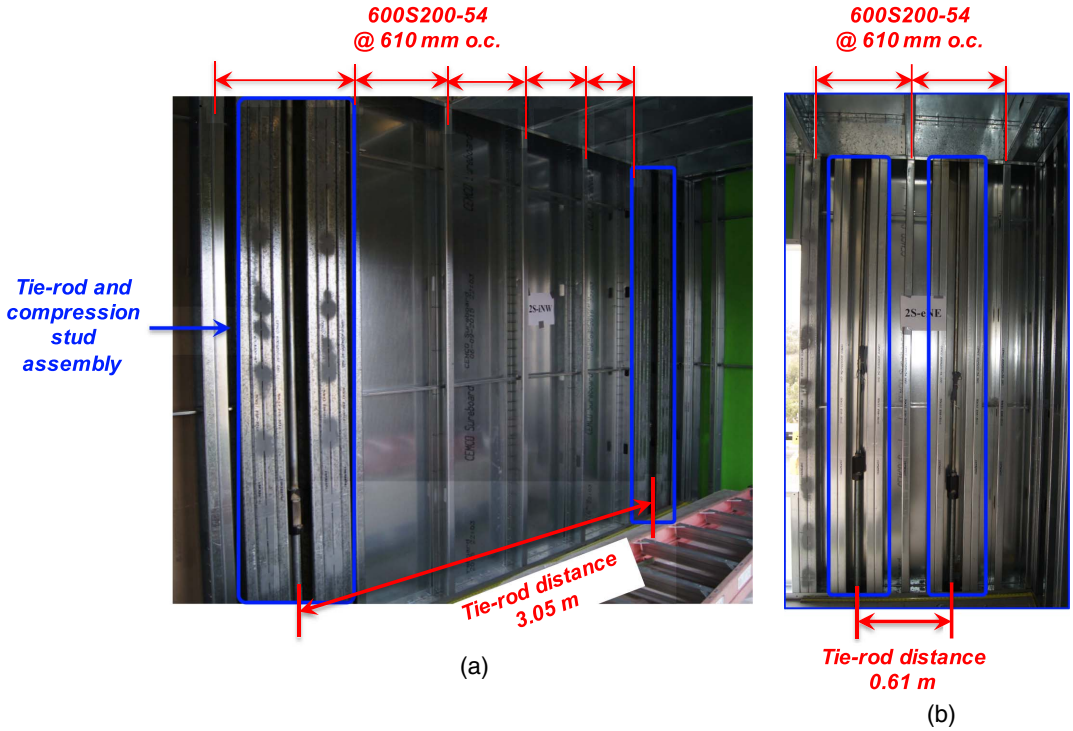

Fig. 2. Shear wall framing at Level 2: (a) corridor shear wall (west segment) (adapted from Hutchinson et al. 2021, © ASCE); and (b) longitudinal corner shear wall (northeast segment) (image by Xiang Wang).

These sheathing panels were attached to the corridor wall framing using #8 self-tapping metal screws spaced at 406 mm (16 in.) o.c. in the field and varying boundary (edge) spacing of 76 mm (3 in.) o.c. for the lower three levels, 102 mm (4 in.) for Level 4, and 152 mm (6 in.) o.c. for the upper two levels. In contrast, the screw spacing of the corner shear walls was 152 mm (6 in.) o.c. on the boundary and 406 mm (16 in.) o.c. in the field at all levels. Additional framing details of the corridor and corner shear walls are discussed in the companion paper (Hutchinson et al. 2021).

Wall-End Tension/Compression Assemblies

Tension and compression loads at the ends of each shear wall were resisted using steel tie-rod and compression stud assemblies (Fig. 2). For brevity, these assemblies are referred to as shear wall tie-down assemblies throughout the remainder of this paper. As shown in Fig. 3(a), each tie-down assembly consisted of (1) steel rods connected by couplers and spanned continuously to the adjacent levels, and (2) light-frame compression posts made of built-up stud packs. The steel rods were spliced by high-strength couplers (SAE Grade 8 at the lower four levels and SAE Grade 5 at the upper two levels) with a double-nut configuration placed at roughly 0.6 m (2 ft) above the floor level [Fig. 3(b)].

Specifically, the adjoining rods were tightened mechanically (with no pretension) to the coupler to ensure the vertical continuity of tie-down assembly, and the snug-tightened nuts were spot-welded to the coupler. The use of high strength steel for the couplers ensured that the tensile strength of the couplers was larger than that of their adjoining rods. Additionally, all steel rods were fastened to the floor diaphragm using the ASTM A36 (ASTM 2019) bearing plate with dimensions of 203 mm (8 in.) × 114 mm (4.5 in.) × 38 mm (1.5 in.) and Society of Automotive Engineers (SAE) Grade 5 washer connections [Fig. 3(c)]. The distance between the tie-rod pair of the exterior (corner) shear walls in the longitudinal direction was ∼0.6 m (2 ft), resulting in an aspect ratio >4:1 considering a clear wall height of ∼2.8 m (9 ft 2 in.) excluding the diaphragm thickness [Fig. 2(b)]. In contrast, the tie-rod pair distance was ∼3.0 m (10 ft) for the west corridor wall segments and ∼2.4 m (8 ft) for the east corridor wall segments [Fig. 2(a)]. Therefore, the aspect ratio of the corridor shear walls was approximately 1:1.

Two different types of steel rods were used for the tie-down assemblies: (1) all-thread rods, and (2) smooth rods with threading at the rod ends (colloquially referred to as Z-rods). These steel rods were fabricated using either ASTM A36 (ASTM 2019) (plain finish) or ASTM A193 (ASTM 2020) Grade B7 (zinc-coated) steel, respectively. Due to the differences in the vertical force demands of the tie-down assemblies for individual shear walls, the steel rods (e.g., steel grade and diameter) and the compression stud packs (e.g., quantity and framing members of the vertical studs) varied depending on their vertical and planar locations. Per ASCE 7 provisions (ASCE 2016), the steel rods and compression studs were designed with an overstrength factor Ω_o of 3.0 applied to the shear wall design strength to ensure sufficient reserve capacity for these critical structural elements. As a result of their much smaller shear capacity, the tie-down assemblies embedded within the exterior shear walls were constructed using tie rods with smaller diameters and smaller compression stud packs in comparison with those of the interior corridor shear walls at the same levels. Detailed specifications of the shear wall tie-down assemblies of the instrumented shear walls at the three select levels, namely Levels 1, 2, and 4, are summarized in Table 1. Fig. 1 of the companion paper shows the specific level numbers of the test building (Hutchinson et al. 2021).

Shear Wall Instrumentation

Seventeen shear walls were instrumented at the three select levels of the test building, namely Levels 1, 2, and 4. As shown in Fig. 4(a), the lower two levels each included three corridor (interior) shear

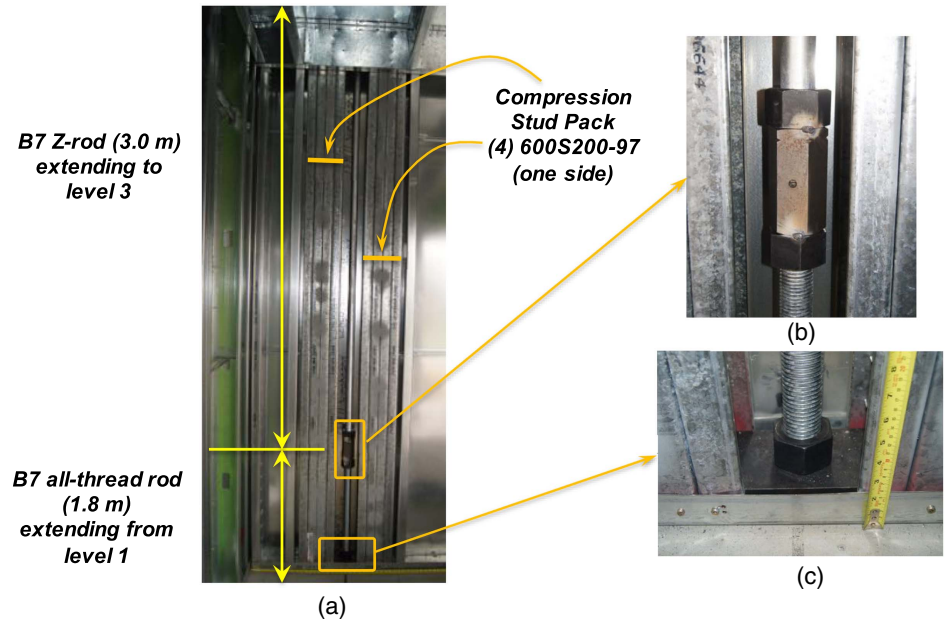

Fig. 3. Tie-down assembly details of the Level 2 corridor shear wall: (a) overall view; (b) coupler and double-nut connection; and (c) bearing plate and washer connection (embedded into the bottom track). (Images by Xiang Wang.)

Table 1. Specifications of the steel rods and compression stud packs at levels 1, 2, and 4

	Corridor (interior) shear wall					Corner (exterior) shear wall				
	Steel tie rod					Steel tie rod				
Level	ASTM designation	f_u (f_y) (MPa)	ø (mm)	F_u (F_y) (kN)	Compression stud pack	ASTM designation	f_u (f_y) (MPa)	ø (mm)	F_u (F_y) (kN)	Compression stud pack
1	A722 (Grade 150) (ASTM 2018)	1,034 (827)	46	1,721 (1,374)	(10) 600S200-97	A722 (Grade 150)	1,034 (827)	46	1,721 (1,374)	(4) 600S200-68
2	A193 (Grade B7) (ASTM 2020)	862 (724)	43	1,250 (1,051)	(8) 600S200-97	A36	400 (250)	29	265 (165)	(4) 600S200-54
4	A193 (Grade B7)	862 (724)	29	569 (478)	(8) 600S200-97	A36	400 (250)	19	114 (71)	(4) 600S200-54

Note: f_u = ultimate stress; f_y = yield stress; ø = nominal diameter of steel rod; F_u = ultimate strength; F_y = yield strength; and Young's modulus of all steel rods is assumed as 200 GPa.

walls (denoted as SW-*c*, SE-*c*, and NW-*c*) and three corner (exterior) shear walls (denoted as SW-*e*, SE-*e*, and NE-*e*), and Level 4 consisted of five instrumented walls because the northeast corner shear wall was not instrumented due to difficulties related to the wall exterior accessibility. Fig. 4(b) schematically illustrates the typical analog sensor plan for an individual shear wall segment. Each wall segment consisted of the following two types of sensors: (1) displacement transducers (i.e., string potentiometers and linear potentiometers) on the shear wall panels, and (2) strain gauges on the steel tie rods. Data recorded by these sensors provided local responses of the shear walls in the following three categories:

1. Sheathing panel shear distortion: measured using two diagonal and two vertical string potentiometers placed in a double-triangle configuration. Because these string potentiometers were directly attached to the structural panels rather than the wall framing, the measurements from these sensors represented the shear distortion, i.e., the angular distortion of the triangles of the shear wall structural panels. The shape (edge lengths) of the triangles varied as a result of the difference of the shear wall lengths.
2. Tie-rod axial forces: measured using a pair of colocated strain gauges (or a single strain gauge) on the tie rods. Because the steel rods all remained elastic during the earthquake tests (as confirmed later in the "Shear Wall Local Seismic Responses" section), the axial force of a tie rod is calculated by multiplying the measured strain of the tie rod by its axial stiffness (product of effective sectional area and Young's modulus of the steel rod). Because the axial force demands of all tie rods remained well below the corresponding yield strength during all earthquake tests (discussed subsequently), the tie-rod forces are all determined with an assumed Young's modulus of 200 GPa in the absence of material testing of the steel rods.
3. Wall end vertical displacements: measured directly using two vertically oriented linear potentiometers at the base of the wall (one sensor at each wall end).

Summary of Test Protocol and Building Response

The multihazard test program consisted of three separate test phases, namely prefire earthquake, postearthquake fire, and postfire earthquake, respectively. The building was subjected to seven earthquake tests of increasing motion intensity during the prefire earthquake test phase (EQ1–EQ7). Earthquake motions were scaled to impose service, design, and maximum considered earthquake (MCE) demands onto the test building. The peak interstory drift ratios (PIDRs) increased from ~0.1% during the service-level earthquake test

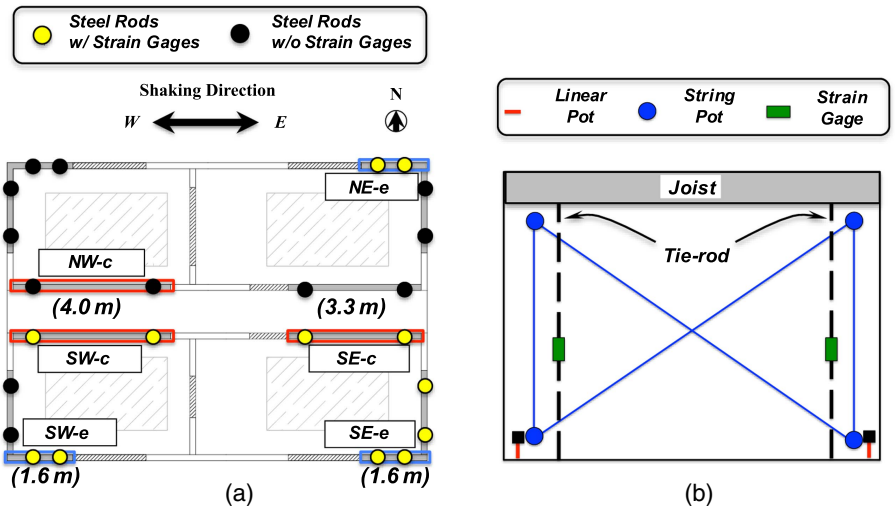

Fig. 4. Shear wall instrumentation plan: (a) location of instrumented shear walls typical of Levels 1, 2, and 4 (wall length specified in the parenthesis); and (b) typical shear wall sensor configuration.

sequence (EQ1–EQ3) to ~0.7% during the design event test (EQ6) and exceeded 1.5% during the MCE test (EQ7). The shear wall system at all levels of the building performed satisfactorily during the prefire earthquake tests. Typical damage of the shear walls involved extensive screw withdrawal and sheathing crushing at the wall boundaries, as well as local buckling steel sheathing of the structural panels.

Subsequently, live fire tests were conducted on the earthquake-damaged building at Levels 2 and 6. The elevated compartment temperatures caused significant degradation of the wall sheathing. Finally, the postfire earthquake test sequence involved a service-level aftershock event (EQ8) and a near-fault extreme event (EQ9). The service-level aftershock test (EQ8) introduced no additional damage to the test building as a result of the very low seismic drift demands (PIDR < 0.2%). Nevertheless, the final near-fault extreme event (EQ9) induced excessively large drift demands at Level 2 of the test building (PIDR > 12% and residual drift of ~6%) and consequently resulted in extremely severe damage to the structural system at this level. Detailed discussions of the overall test protocol and the building global responses are available in the companion paper (Hutchinson et al. 2021).

Shear Wall Local Seismic Responses

The measured shear wall local responses are investigated in this section to understand the seismic behavior of individual shear walls as well as their system-level interactions during the earthquake tests. The following two aspects are considered as the major variables of the shear walls in the test building: (1) shear wall with varied details (corridor shear wall versus exterior shear wall), and (2) location along the building height (differences in story force and drift demands). Discussion of the shear wall behavior first focuses on understanding their response characteristics by correlating the local responses of individual shear walls with the global story drift responses, and subsequently, the peak local responses of different shear walls during the prefire and postfire earthquake tests are summarized and compared.

Local Response Histories: Design Event Results

The measured local responses of the shear walls, when compared and contrasted in the time domain, reveal important behavior characteristics in response to the story drift demands as well as the interactions of individual shear walls (e.g., corridor walls placed along the same wall line and corridor and exterior shear walls at the same quadrant). In this regard, the time-history responses of the Level 2 corridor (SW-*c* and SE-*c*) and exterior (SW-*e* and SE-*e*) shear walls during the design event (EQ6) are presented herein to illustrate their response characteristics. To correlate the global responses with the shear wall local responses, the story drift and story shear of level 2 during the design event (EQ6) are presented in Fig. 5.

It is noted that the circles as annotated in the response history plots denote the time instances when the story drift achieved the peak values in the positive (eastward) and negative (westward) directions. These circles are consistently presented in the shear wall

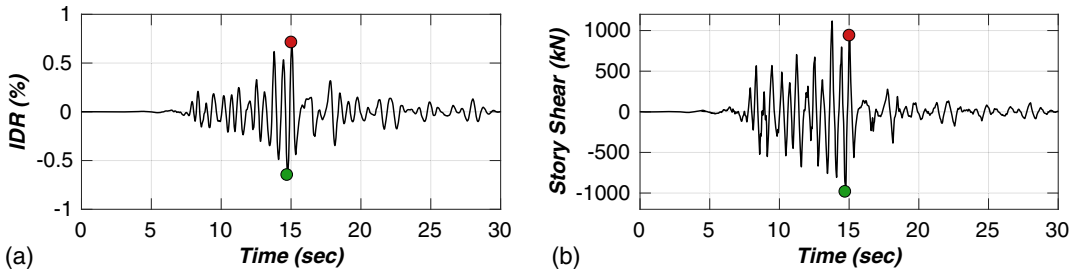

Fig. 5. (a) Level 2 story drift; and (b) story shear responses during the design event (EQ6). Circles denote the time instances of the Level 2 peak story drift in the positive (eastward) and negative (westward) directions.

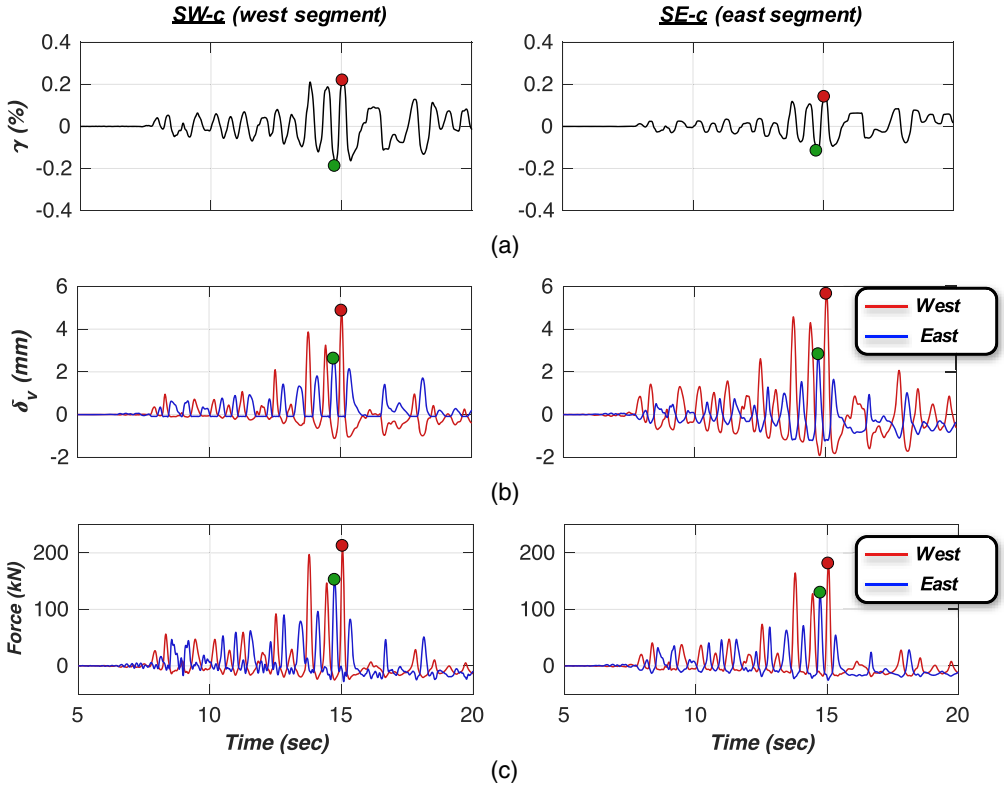

Fig. 6. Local responses of the corridor shear wall pair at level 2 during the design event (EQ6): (a) panel shear distortions; (b) wall end vertical displacements; and (c) tie-rod axial forces. Circles denote the time instances of the Level 2 peak story drift in the positive (eastward) and negative (westward) directions.

local response histories. As shown in Fig. 5, Level 2 reached the peak story drift of 0.7% in the positive (eastward) direction and 0.65% in the negative (westward) direction during the design event (EQ6). The story shear associated with both the positive and negative peak story drifts were nearly 1,000 kN.

Fig. 6 shows the measured local responses of the corridor shear wall pair (SW-*c* and SE-*c*) at Level 2 during the design event (EQ6). The circles as shown in the time-history responses indicate that the occurrences of the peak shear distortion on the sheathing panels coincided with those of the corresponding story drift response. Comparison of results reveal that the local responses of the west and east wall segments appeared highly coincidental and attained comparable peak values in response to the story drift demands. With a peak story drift of ~0.6% at Level 2, the peak shear distortion of the sheathing panels attained ~0.2% for SW-*c* (west segment) and ~0.15% for SW-*e* (east segment).

As the story drift of Level 2 reached the positive (eastward) peak, the wall end vertical displacements and the tie-rod tensile forces of both corridor wall segments (SW-*c* and SE-*c*) achieved their peak values at the west ends of the wall segments, whereas these responses remained small at the east ends. This is due to the fact that the east end of each wall segment was subjected to compressive axial force when imposed to its peak story drift in the positive (eastward) direction.

Similarly, when the story drift reached the negative (westward) peak, the peak wall end vertical displacements and peak tie-rod tensile forces of both corridor wall segments occurred at the east ends of the shear walls. The tie rods of both wall segments achieved peak tensile forces of ~200 kN at the instance of the positive (eastward) peak story drift and <150 kN at the instance of the negative (westward) peak story drift. The peak tensile forces in the tie rods were well below (~20%) their yield strength of 1,051 kN (Table 1) during the design event (EQ6). This anticipated small axial force ratio is attributed to the use of an overstrength factor Ω_o of 3.0 for the tie-rod design, which precludes attainment of capacity in these essential elements during the earthquake loading.

Fig. 7 shows the measured responses of the longitudinal corner (exterior) shear wall pair (SW-*e* and SE-*e*) at Level 2 during the design event (EQ6). These corner shear walls were much more slender than the corridor walls because their aspect ratio (height over wall length) exceeded 4:1 [Fig. 2(b)]. Because the shear force demands attributed to these short exterior shear walls were much smaller than those of the corridor shear walls, the peak shear distortions (~0.1%) and peak wall end vertical displacements (<2 mm) of the corner shear walls were smaller than those of the corridor walls. Similarly, the occurrences of these local peak responses coincided with those of the peak story drift at Level 2. Furthermore, the peak axial forces of the corner wall tie rods were substantially smaller than those of the corridor walls (slightly larger than 60 kN). However, the peak axial force ratio (~40% given the yield strength of 165 kN) was higher than those of the corridor wall tie rods because the corner wall tie-rod diameter was much smaller than those of the corridor walls (Table 1).

Shear Wall Interaction Behavior

Because the shear wall tie rods are critical structural elements within the uplift restraint system, knowledge of their axial forces is essential for understanding the interaction among individual shear walls. Fig. 8 illustrates the planar distribution of the tie-rod axial forces of the Level 2 corridor and corner shear walls associated with the peak story drift during the design event EQ6 [Fig. 5(a) shows the

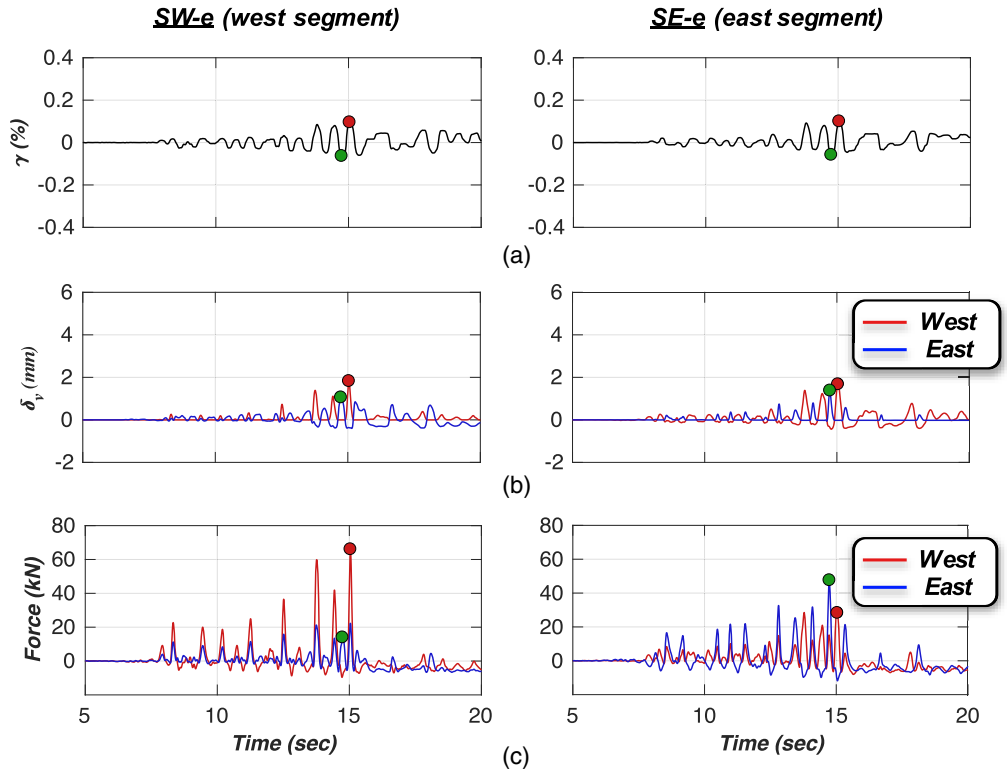

Fig. 7. Local responses of the longitudinal corner shear wall pair at Level 2 during the design event (EQ6): (a) panel shear distortions; (b) wall end vertical displacements; and (c) tie-rod axial forces. Circles denote the time instances of the Level 2 peak story drift in the positive (eastward) and negative (westward) directions (red–positive; green–negative).

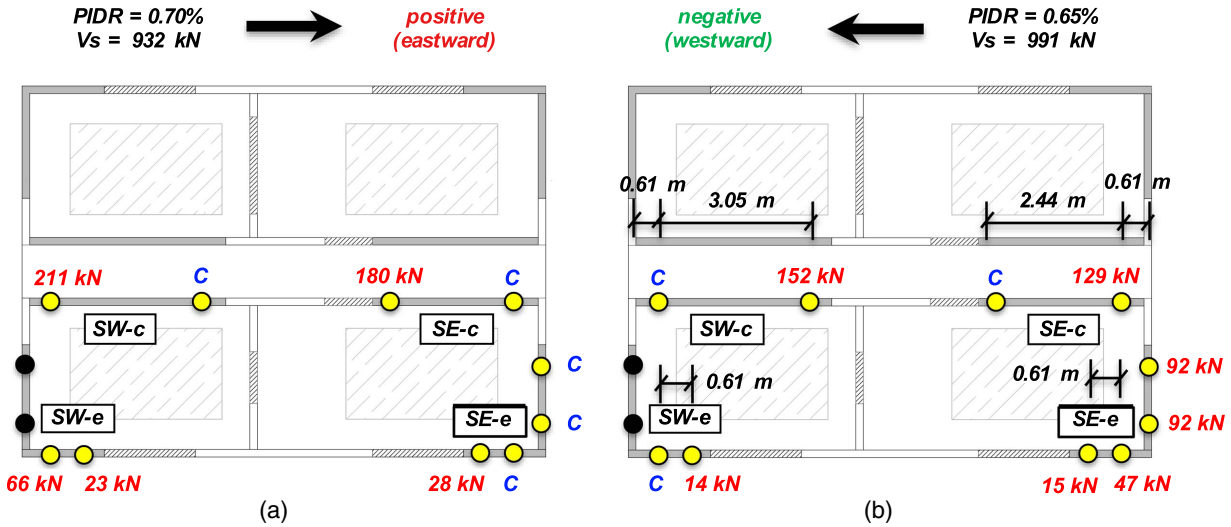

Fig. 8. Tensile force distribution of the Level 2 shear wall tie rods during the design event (EQ6): (a) positive peak story drift; and (b) negative peak story drift. C denotes that the tie rod was subjected to compression. Note that the tie rods of the transverse walls at the southwest corner were non-instrumented.

story drift response]. The achieved tie-rod tensile forces were comparable between the two corridor walls (SW-*c* and SE-*c*) in both the positive and negative loading directions. Importantly, the attainment of peak tensile force within the tie rod at one end of a corridor wall segment consistently corresponded to a compressive force of the tie rod on the other end of the wall segment. These observations indicate that the corridor shear walls performed as independent wall segments, i.e., Type I systems per AISI code provisions (AISI 2015a, b) in response to earthquake loading.

In contrast, the correlation of the tie-rod axial forces between the exterior shear walls (SW-*e* and SE-*e*) appear less consistent than the corridor shear walls. When the positive (eastward) peak story drift of 0.7% occurred at Level 2 [Fig. 8(a)], the tie-rod pair of the west segment (SW-*e*) was both subjected to tensile forces (66 and

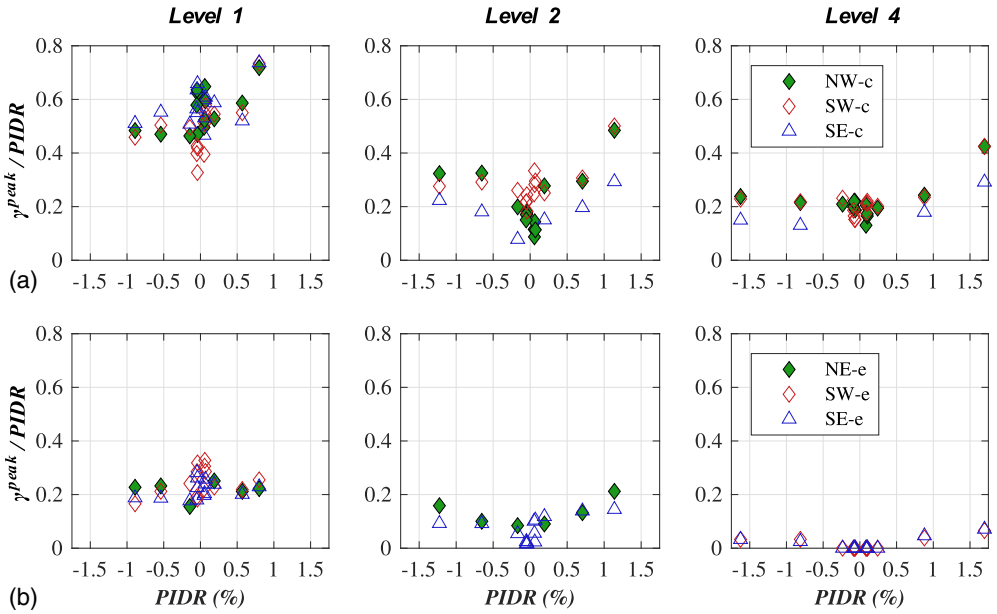

Fig. 9. Normalized peak panel shear distortions of the (a) corridor; and (b) corner shear walls during the prefire earthquake test sequence.

23 kN). The east wall segment (SE-*e*) underwent similar behavior in the occurrence of the negative (westward) peak story drift of 0.65%, with tensile forces of 47 and 15 kN for both tie rods [Fig. 8(b)]. Indeed, the exterior wall tie rods (both the longitudinal and transverse walls at the southwest corner) were all subjected to tensile forces in the occurrence of the negative (westward) peak story drift [Fig. 8(b)]. This force distribution pattern occurred consistently for the Level 1 shear wall tie rods, although the results are not shown for brevity. Such tie-rod force distributions are indicative of the interaction between the interior corridor shear wall (SE-*c*) with the adjacent exterior transverse and longitudinal walls (SE-*e*) via the kinematic constraints provided by the floor diaphragm.

The tie-rod tensile forces of the Level 2 shear walls are subsequently correlated with the story shear associated with the negative story drift [Fig. 8(b)]. It is assumed that the tensile forces of all southeast shear wall (SE-*c* and SE-*e*) tie rods were equilibrated by the tie-down assembly at the west end of the corridor wall SE-*c* (denoted with C) because it served as the structural element designated to sustain compressive loads. Additionally, the tensile forces of the southwest shear walls (SW-*c* and SW-*e*) tie rods were each equilibrated by the tie-down assembly at the west end of the shear wall. For instance, the tie-rod tensile force of 129 KN at the east corridor wall (SE-*c*) with a distance of 2.44 m from the compression center produced a shear force of 103.2 kN considering a story height of 3.05 m. As a result, the total story shear of Level 2 as derived using the assumed equilibrium between the tie-rod tensile forces and compressive forces of the stud packs amounts to ~977 kN, which is consistent with the story shear of 991 kN while at the negative peak story drift [Fig. 5(b)]. Although the locations of the shear wall compressive loads were presumptive rather than explicitly known, the tie-rod axial force and story shear correlation further corroborates the interaction mechanism between the interior corridor shear wall (SE-*c*) and the adjacent exterior walls (SE-*e*) at the corner.

Synthesis of Peak Local Responses: Prefire Earthquake Tests

Fig. 9 shows the ratios of the peak shear distortions of the shear wall sheathing panels normalized by the PIDRs at the corresponding levels. The positive or negative peak shear distortions are correlated with the peak story drifts in the corresponding directions. Comparisons between the corridor walls and the corner walls indicate that the peak shear distortions of the corridor walls were consistently larger than those of the corner walls at the same level. The sheathing panel shear distortions accounted for 20%–40% of the drift demands for the corridor walls at Level 2 but only about 20% for the corner walls. This may be attributed to the differences related to shear wall aspect ratios between the corridor and corner shear walls. The corner shear walls, which were much more slender than the corridor shear walls, may lead to increased flexural deformation and reduced shear deformation contribution in response to lateral seismic loads.

In addition, the shear distortion ratios of the shear walls appeared to be smaller at Level 4, although the story drift demands consistently achieved its largest value at Level 4 during all prefire earthquake tests (PIDR attained ~0.9% at Level 4 compared with ~0.7% at Level 2 during the design event EQ6). The shear distortions of the corridor wall sheathing panels accounted for 40%–60% of the story drift at Level 1 in comparison with 20%–40% at Level 4. This is likely attributed to the axial force demands of the tie rods because the measured tensile forces of the tie rods of the Level 4 shear walls were significantly smaller than those of the lower two levels.

Fig. 10 summarizes the measured peak tensile forces of the corridor and corner shear wall tie-down rods during the prefire earthquake test phase. The tie-down rod axial forces of the northwest corridor shear walls were not measured because no strain gauges were installed on these walls. Data points associated with the positive (eastward) PIDRs represent those of the measured peak tensile forces of the tie-down rods at the west ends of individual shear walls, whereas those associated with the negative (westward) PIDRs represent the peak tensile forces of the tie-down rods at the east ends of the shear walls. As a result of larger lateral force demands at the lower two levels, the measured peak tensile forces of the shear wall tie-down rods at the lower levels were much larger than those of the Level 4 shear walls. The axial forces of the corridor walls at the lower two levels achieved ~400 kN but only 200 kN at Level 4.

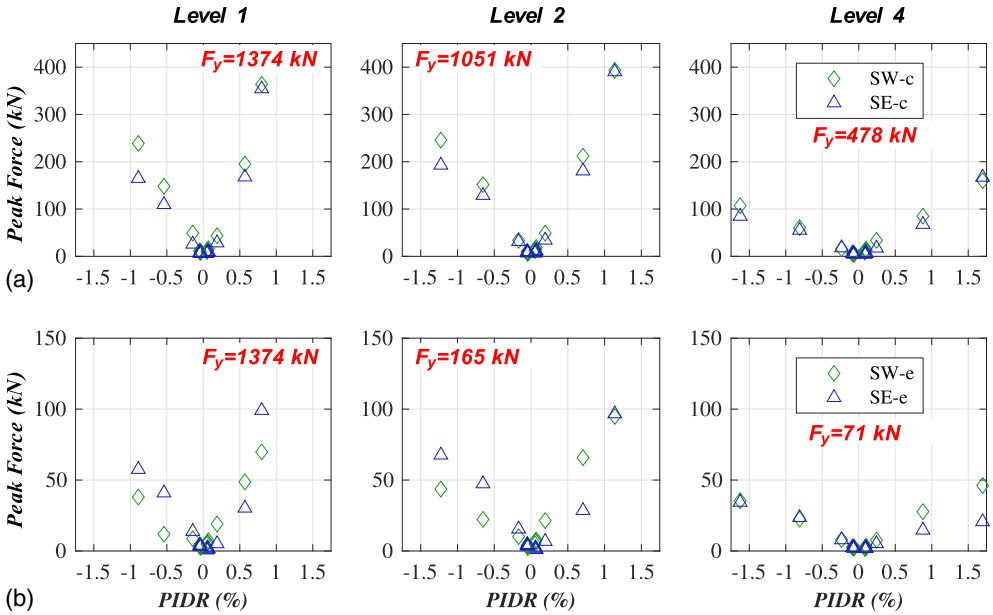

Fig. 10. Peak tie-rod tensile forces of the (a) corridor; and (b) corner shear walls during the prefire earthquake test sequence.

In addition, the peak tensile forces of the corridor shear wall tie-down rods were much larger than those of the corner shear walls at the same level. The achieved peak tensile forces remained comparable for the corridor shear wall pairs (east and west wall segments) for each of the three levels, whereas the forces differed apparently for the corner shear wall pairs. It is also important to point out that the measured axial forces of all instrumented tie-down rods remained smaller than their respective yield strengths. During the prefire test phase, the tensile forces within the corridor shear wall tie rods reached only ~40% their respective yield strength, whereas those of the corner shear walls attained about 60%.

Fig. 11 summarizes the peak wall end vertical displacements of the corridor and corner shear walls during the prefire earthquake test phase. Data points associated with the positive (eastward) PIDRs represent the peak vertical displacements of the west ends of walls, whereas those associated with the negative (westward) PIDRs represent the peak vertical displacements of the east wall ends. As a result of larger tensile force demands of the tie rods at the lower two levels, the vertical (uplift) wall end displacements of the shear walls at these two levels appeared considerably larger than those at Level 4. The peak vertical wall end displacements exceeded 10 mm at the lower two levels in comparison with 2 mm for those of the Level 4 shear walls. In addition, the peak vertical displacements of the corridor shear walls were consistently larger than those of the corner shear walls at the corresponding levels, which is likely attributed to the larger tensile force demands associated with the corridor wall tie rods.

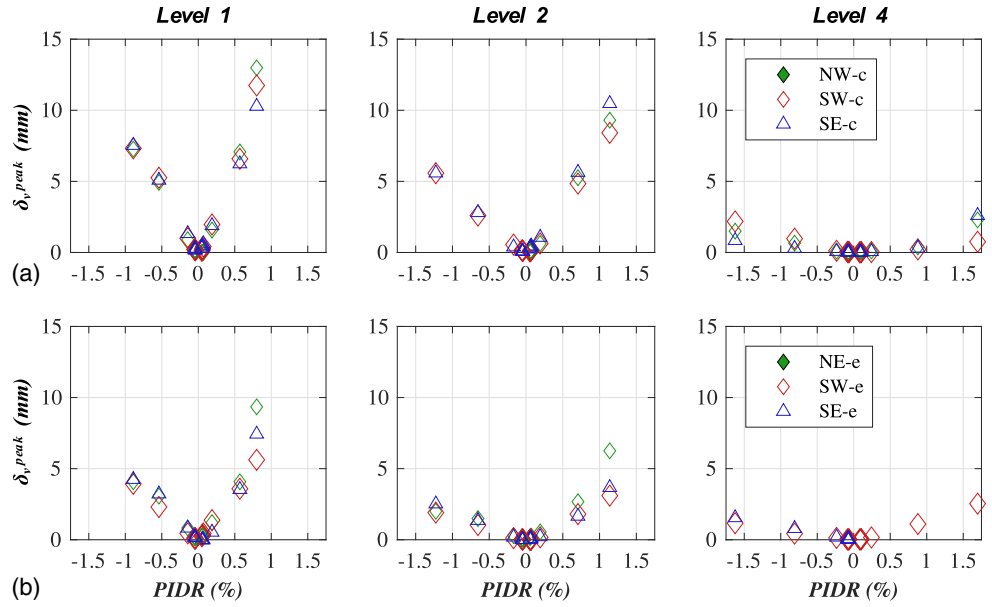

Fig. 11. Peak wall end vertical displacements of the (a) corridor; and (b) corner shear walls during the prefire earthquake test sequence.

J. Struct. Eng., 2021, 147(9): 04021126

Shear Wall Local Responses: Postfire Earthquake Tests

As a result of fire-induced damage to the shear wall sheathing panels at Level 2, the final near-fault extreme event test (EQ9) induced excessively large drift demands at this level (peak interstory drift exceeded 12% and residual interstory drift reached ~6%) and resulted in extremely severe structural damage to the Level 2 shear walls. In this regard, this subsection focuses on presenting the shear wall local responses during the final postfire MCE level test (EQ9) and compares the peak local responses with those achieved during the prefire MCE test (EQ7). Although the input motions of these two MCE level tests adopted different seed records, these motions were amplitude-scaled to provide comparable spectral acceleration demands within the building fundamental period range (Wang et al. 2016).

Fig. 12 shows the tie-rod axial forces of the southeast corridor and corner walls (SE-*c* and SE-*e*) [Fig. 4(a)] during the postfire MCE level test (EQ9) at the three instrumented levels (i.e., Levels 1, 2, and 4) as well as the Level 2 corner wall (SE-*e*) connection failure at the end of the test program. The interstory drift ratio (IDR) response of Level 2 is also included in the figure. Similar to their behavior characteristics during the prefire earthquake tests, the peak tensile forces of the corridor shear wall tie rods coincided with the occurrences of the peak story drifts at the corresponding levels. Despite the large seismic drift demands during this test (e.g., PIDR exceeded 12% at Level 2), the peak tensile forces of the corridor wall tie rods at the three levels remained lower than 50% of their nominal yield strength (Table 1).

Importantly, the west end tie-rod tensile forces of the corner walls (SE-*e*) at all three levels underwent simultaneous and abrupt drops slightly before the occurrence of the positive (eastward) peak story drift of 12% at Level 2 but remained almost constant thereafter. This behavior was attributed to the failure of a coupler connecting the west end tie rods of the southeast corner wall at Level 2 [Fig. 12(b)]. This connection failure represented the only instance of its kind during the entire test program. Axial force redistribution

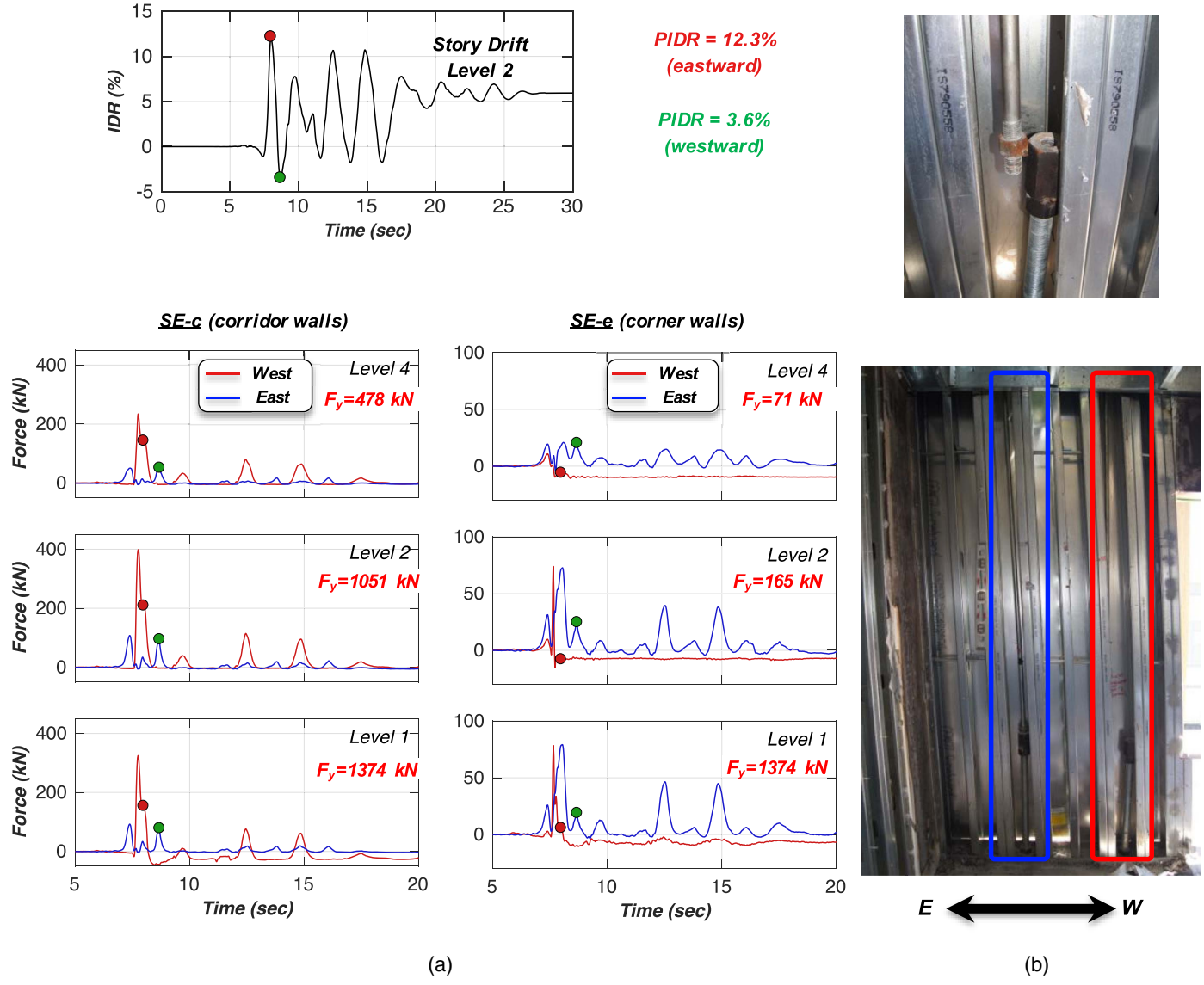

Fig. 12. (a) Tie-rod axial force histories of the southeast corridor and corner shear walls (SE-*c* and SE-*e*) during the postfire MCE test (EQ9); and (b) corner shear wall tie-rod (*SE-e*) connection failure at the end of the test program. Circles denote the time instances of the Level 2 peak story drift in the positive (eastward) and negative (westward) directions. The arrow indicates the direction of shaking (images by Xiang Wang).

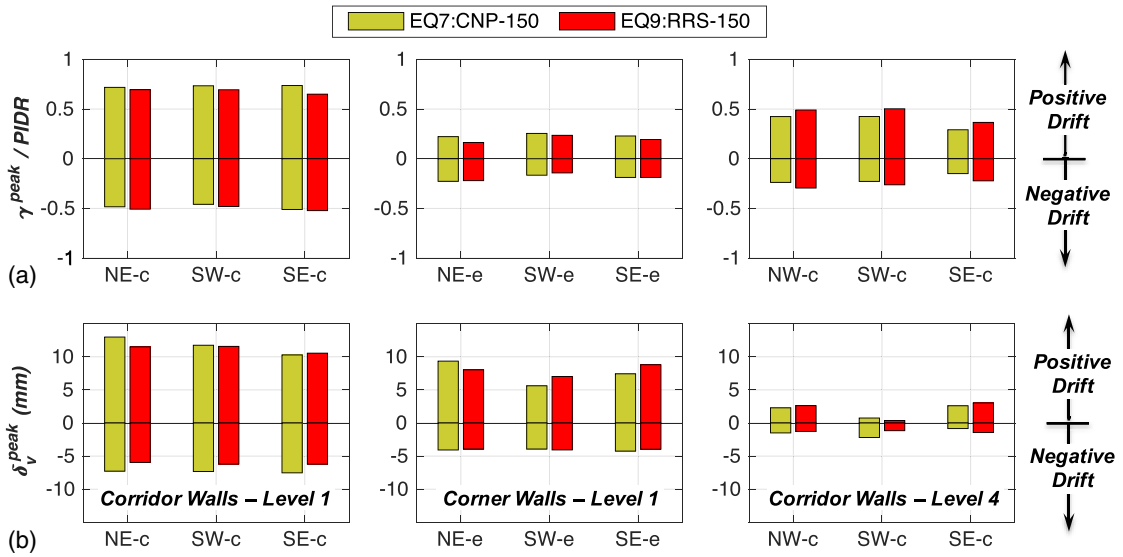

Fig. 13. Comparison of (a) peak sheathing panel shear distortion ratios; and (b) peak wall end vertical (uplift) displacements of select shear walls during the prefire and postfire MCE level tests (EQ7 and EQ9).

occurred following the loss of tensile capacities of the west end tie rods, which is substantiated by the appreciable increase of tensile forces for the east end tie rods in response to the positive (eastward) drift demands. Because the disconnected tie rod was only subjected to a tensile force demand of ~70 kN prior to the failure, which was well below its nominal yield strength of 165 kN, it is likely that this failure was induced by the large story drift demands imposed on the tie-rod connection (>12% story drift at Level 2). Therefore, further studies are recommended to evaluate the tie-rod connection behavior under extreme drift demands.

Fig. 13 compares the sheathing panel peak shear distortion ratios and peak wall end vertical (uplift) displacements of select shear walls during the prefire and postfire MCE level tests (EQ7 versus EQ9). The west wall end uplift displacements were associated with the positive (eastward) story drifts, whereas those of the east wall ends correspond to the negative (westward) story drifts. Because the displacement transducers at certain locations were removed prior to or damaged during the fire tests, comparison of the local responses focuses on the corridor and corner shear walls at Level 1 and the corridor shear walls at Level 4. Although the story drift demands of these two levels achieved during the postfire MCE test (EQ9) were moderately larger than those of the prefire MCE test (EQ7), both the peak shear distortion ratios and wall end uplift displacements of the shear walls attained during the postfire MCE test remained comparable to the corresponding prefire counterparts. The uplift displacements of the Level 1 corridor shear walls were substantially larger uplift displacements than those at Level 4 as a result of larger tie-rod force demands. In addition, the uplift displacements of the corridor shear walls at Level 1 were slightly larger than those of the corner shear walls at the same level.

Seismic Design Parameters Inferred from Experimental Data

This section focuses on exploring the seismic behavior of the test building in relation to present design and analysis approaches adopted for CFS shear wall structures. With the assumption that the test building performed as a linear system during the prefire service-level earthquake sequence (EQ1–EQ3) due to the low story drift demands (<0.1%), its dynamic characteristics during these tests are determined using a parameter optimization strategy (Cruz and Miranda 2016, 2019). Subsequently, the measured global force and displacement responses at various performance levels (i.e., from service-level design to MCE) are employed to infer key seismic design parameters of the CFS test building. Importantly, the implications of the experimentally inferred parameters are discussed and compared with current design provisions and guidelines (e.g., BSSC 2015; ASCE 2016).

Building Dynamic Characteristics during Service-Level Earthquake Tests

The test building was assumed to perform as a linear system during the service-level earthquake test sequence (EQ1–EQ3) as a result of the low seismic drift demands (<0.1%). Accordingly, a time-domain optimization method proposed by Cruz and Miranda (2016, 2019) is employed herein to determine the building periods and damping ratios associated with these low-amplitude earthquake tests. The optimization method adopts the modal superposition principle for reconstructing the building dynamic responses during the earthquake tests and subsequently extract the modal parameters of the building by minimizing the error metric (objective function) between the measured floor responses and those reconstructed via modal superposition.

In this study, the objective function $J(\theta)$ is defined as the differences between the predicted (relative) floor acceleration $\tilde{a}_i(t)$ and the measured (relative) floor acceleration $a_i(t)$ normalized by the measured floor acceleration summed over the significant motion duration $D_{s,5-95}$ (Kramer 1996) for all floors, which is also referred to as relative root-mean square error (RRMSE) of the floor acceleration

$$J(\theta) = \frac{1}{N}\sum_{i=2}^{n_f}\sqrt{\frac{\sum_{t=D_{s,5}}^{D_{s,95}}[a_i(t)-\tilde{a}_i(t)]^2}{\sum_{t=D_{s,5}}^{D_{s,95}}[a_i(t)]^2}} \quad (1)$$

where N = total number of floors where measured floor accelerations are available ($N = 6$ in this study); n_f = total floor number (summation over floor starts from the second floor because the

acceleration at the first floor is considered as the input excitations for the modal analysis); and $D_{s,5}$ and $D_{s,95}$ = time instances when the earthquake input motion reaches 5% and 95% Arias intensity (Arias 1970). To minimize the objective function $J(\theta)$, the proposed optimization method considers the modal parameters θ of a total of m modes that are sufficient for the modal analysis

$$\theta = \begin{Bmatrix} T_1 & \varepsilon_1 & \begin{bmatrix} \Gamma_1\phi_{11} & \cdots & \Gamma_m\phi_{1m} \\ \vdots & \ddots & \vdots \\ \Gamma_1\phi_{n1} & \cdots & \Gamma_m\phi_{nm} \end{bmatrix} \\ \vdots & \vdots & \\ T_m & \varepsilon_m & \end{Bmatrix} \tag{2}$$

where T_i, ε_i, and Γ_i = period, damping ratio, and modal participation factor associated with the ith mode; and ϕ_{ji} = modal shape component at the jth floor for the ith mode.

To determine the proper number of modes and initialize the optimization parameters, a time-domain input-output system identification method, namely the deterministic-stochastic identification (DSI) method (Van Overschee and De Moor 1996), is employed to estimate the modal parameters of the test buildings (i.e., periods, damping ratios, and mode shapes) using floor acceleration responses recorded during the white-noise tests. Specifically, the system input and output involve the measured longitudinal accelerations of the shake-table platen and each floor of the test building, respectively. Additionally, the floor mass distribution of the building is considered explicitly known because the building weight determined by hand calculation agrees reasonably well with the measured gravity loads of the building (Wang et al. 2016).

Using the white-noise data recorded at the beginning of the earthquake test phase, i.e., corresponding to the initial state of the building, the first and second longitudinal modes of the building are identified using the system identification method (Wang and Hutchinson 2020). The mode shapes and the associated modal parameters of these identified modes are presented in Fig. 14. Because the cumulative effective modal mass of the first two longitudinal modes exceeds 98% of the total building mass, the modal superposition analysis is considered sufficient accounting for only these two vibration modes. To further reduce the parameters of the optimization problem, the mode shapes extracted from the white-noise test are considered invariant during the service-level events (EQ1–EQ3) because the system identification results indicate that the mode shapes are much less sensitive than the corresponding periods and damping ratios in response to the variation of excitation amplitudes (Wang and Hutchinson 2020). In this regard, only the periods and damping ratios associated with the first two longitudinal modes are considered as optimization parameters in the present study.

Fig. 15 compares the measured floor accelerations of the test building during the service-level Test EQ2 and the modal superposition results simulated using the initial parameters (as identified from the white-noise test data) and the optimized parameters. This comparison demonstrates the effectiveness of the optimization method in reducing the error metrics between the measured and simulated floor accelerations. The error associated with the objective function (RRSME) drops substantially from an initial value of ~70% to 10% when the optimized modal parameters are used in the modal analysis.

Fig. 16 presents the sensitivity of the objective function (RRMSE between the measured and simulated floor acceleration responses) with respect to the optimization parameters, namely the periods and damping ratios associated with the first two longitudinal modes. Because the minimum of each sensitivity curve

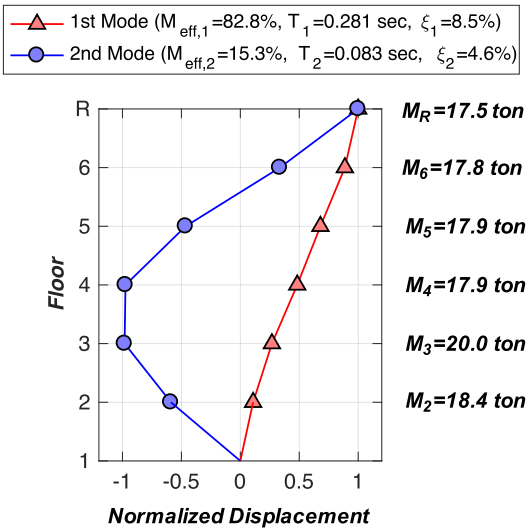

Fig. 14. Modal properties of the first and second longitudinal modes identified using the white-noise data recorded at the beginning of the earthquake test phase.

represents an optimal modal parameter of the building, the optimal period and damping ratio corresponding to Test EQ2 are ~0.33 s and ~10% for the first mode as well as ~0.09 s and ~8% for the second mode, respectively. These results appear reasonable because the building periods and damping ratios obtained from the service-level Earthquake EQ2 are slightly larger than those identified using the white-noise test data as a result of the increased excitation amplitude for the earthquake test (Wang and Hutchinson 2020). Additionally, the objective function (error) appears less sensitive to the change of the modal parameters associated with the second mode. This may be attributed to the relatively small second mode contribution to the total building response in comparison with that of the first mode.

Following the validation effort as described previously, the parameter optimization method is adopted to analyze the periods and damping ratios associated with the first and second longitudinal modes during the service-level test sequence (EQ1–EQ3). As summarized in Table 2, the modal parameters of the building remain consistent among the three low-amplitude earthquake tests, with a variation of ~5% for the periods and 15%–20% for the damping ratios. Per the ASCE 7 code provisions (ASCE 2016), the estimated fundamental period of the building used in the seismic design is calculated as 0.43 s given a building height of 18.3 m (60 ft), representing an overestimation of ~30% compared with those identified from the test data (0.32–0.35 s).

Additionally, the identified damping ratios of both building vibration modes (8%–10%) is 1.5–2.0 times greater than the typical upper bound value of 5% as recommended by the design guidelines (FEMA 2018). Realistic CFS buildings with complete wall finishes and other architectural features are likely to observe even larger damping ratios in comparison with that of the test building, which only consisted of the structural skeleton and nonfinished sheathing (gypsum wall boards). The observed dynamic characteristics of the test building are consistent with the findings from a previous shake-table experimental study of a code-compliant CFS shear wall structure tested with similar sheathing installation conditions (Peterman et al. 2016a). It is therefore recommended that these observations be considered in future CFS building design applications.

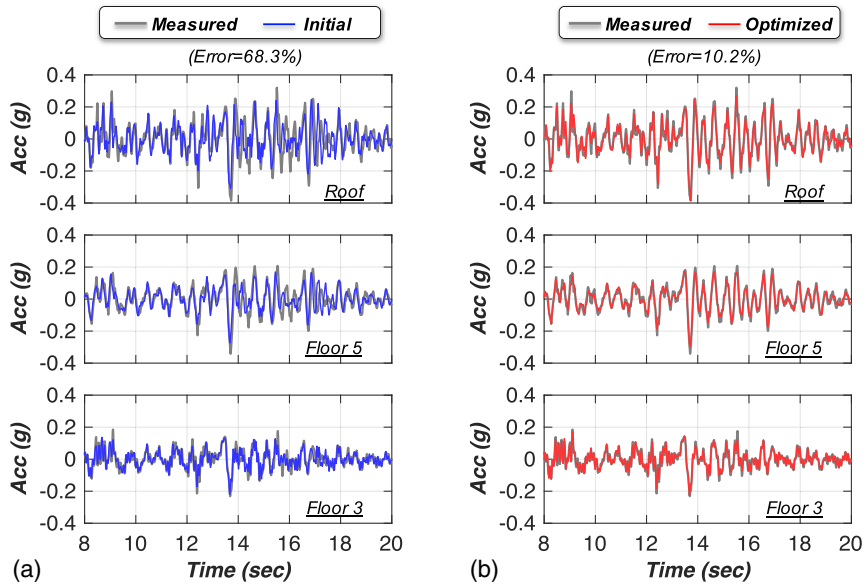

Fig. 15. Comparison of the measured floor accelerations of the test building during Test EQ2 and the modal superposition results simulated using (a) initial modal parameters; and (b) optimized modal parameters.

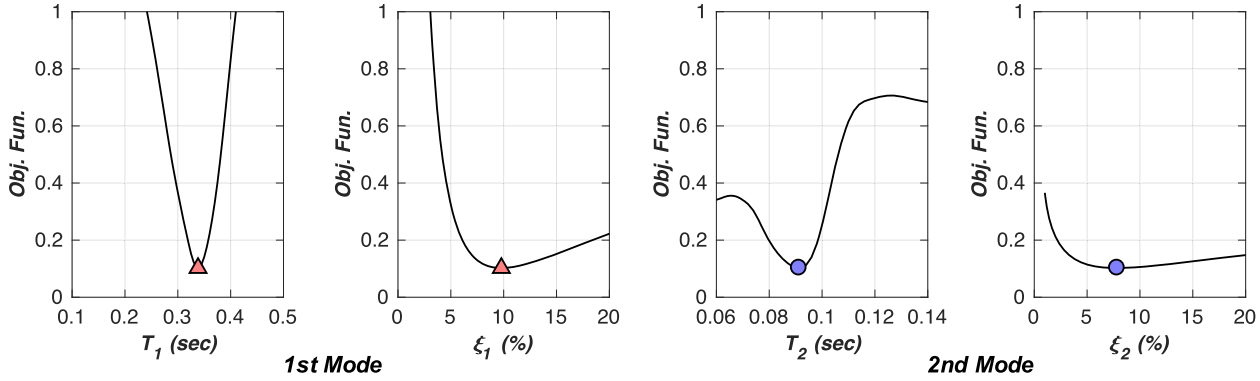

Fig. 16. Sensitivity of the objection function (RRMSE between the measured and simulated floor acceleration responses) with respect to the optimization parameters for Test EQ2. RRMSE denotes relative root-mean square error.

Table 2. Modal parameters of the first and second longitudinal modes during the service-level earthquake test sequence (EQ1–EQ3)

	First mode		Second mode	
EQ test name	Period (s)	Damping ratio (%)	Period (s)	Damping ratio (%)
EQ1:RIO-25	0.325	10.5	0.086	9.7
EQ2:CNP-25	0.338	9.8	0.091	7.9
EQ3:CUR-25	0.348	9.1	0.093	9.2

Seismic Design Factors Inferred from Experimental Data

Among the seven tests during the prefire earthquake test phase, four of them adopt an identical seed motion with gradually increased intensities to achieve distinct performance targets for the test building, namely EQ2:CNP-25 (service level), EQ5:CNP-50 (50% design level), EQ6:CNP-100 (design level), and EQ7:CNP-150 (MCE level). The data collected during these tests provide the opportunity for assessing the seismic design parameters of the test building, namely response modification coefficient R, overstrength factor Ω_o, and deflection amplification factor C_d. In this regard, the seismic design parameters are determined by comparing the measured nonlinear building responses against the surrogate responses of the building upon the assumption of linear response during the earthquake tests. The seismic design parameters utilized in the design process for this building were taken as $R = 6.5$, $\Omega_o = 3$, and $C_d = 4$ per ASCE 7 code provisions (ASCE 2016). Additionally, the design base shear of the building was determined as ~260 kN in consideration of a base shear coefficient C_s of 0.236 and an effective seismic weight W of ~1,160 kN [Wang et al. (2016) and Hutchinson et al. (2021) have provided additional design details].

In this study, the linear surrogate responses of the test building are reconstructed by modal analysis using the measured input (shake-table platen) accelerations during the earthquake tests. The modal parameters employ the optimized results determined using data collected during the service-level Test EQ2 (Fig. 14). Fig. 17 compares the measured roof drift ratio (RDR) and normalized base shear (V_b/W) of the building with the surrogate responses during Tests EQ2 (service level) and EQ6 (design level). The reasonable

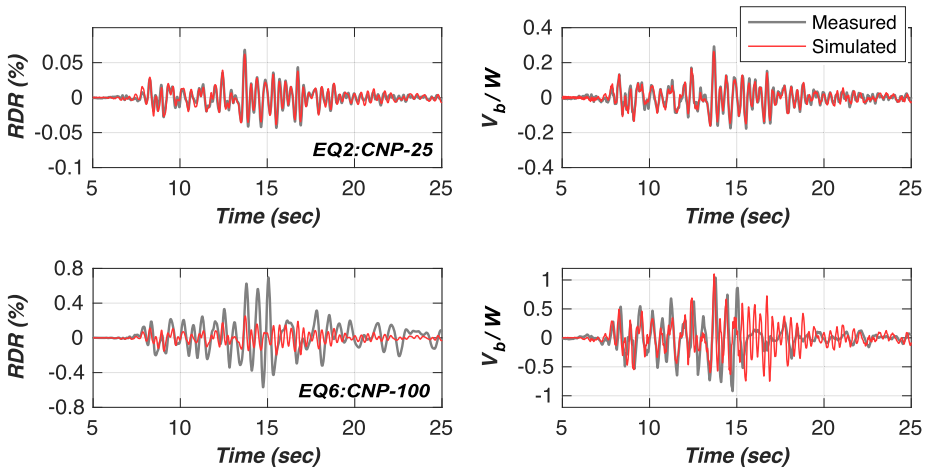

Fig. 17. Comparison among measured roof drift ratio, normalized base shear (V_b/W), and simulated linear responses during Tests EQ2 (service level) and EQ6 (design level).

agreement between the simulated and measured results (<5% peak response errors) during Test EQ2 (service level) corroborates the effectiveness of the modal analysis in replicating the building responses in the linear regime. In contrast, the measured responses of Test EQ6 (design level) differ significantly from the simulated linear responses, highlighting the effect of building nonlinearity on modifying its behavioral characteristics during the design-level test. Although the measured peak base shear is comparable to the surrogate response, the presence of nonlinearity significantly amplifies the roof drift demand because the measured peak roof drift (~0.7%) is roughly three times as much as the simulated peak response (~0.25%). Furthermore, the frequency characteristics of the measured nonlinear roof drift and base shear of Test EQ6 differed substantially from the simulated linear responses as evidenced by the vibration period elongation following the attainment of peak roof drift (at the time instance of ~15 s).

To evaluate the seismic design factors, the measured peak RDR versus normalized base shear responses during four select earthquake tests spanning from service-level to MCE tests, namely EQ2, EQ5, EQ6, and EQ7, are compared with the corresponding linear responses determined using the modal analysis. As shown in Fig. 18, the reference base shear level considered in the seismic design of the test building corresponds to a normalized base shear of 0.29 and a roof drift ratio of ~0.07% (represented by the horizontal dashed line in Fig. 18). These reference force and displacement demands are comparable to those attained during the service-level earthquake test (EQ2). As the motion intensity increased, the test building achieved its peak base shear during the design-level test (EQ6) and underwent no further increase of the base shear demand despite an additional 50% increase of the motion intensity during the MCE test (EQ7). Because the building achieved the peak strength (base shear) during the design-level test (EQ6), the measured building responses during this test and the corresponding linear-elastic responses obtained from the modal analysis are used to evaluate the seismic design factors of the test building as specified in the National Earthquake Hazards Reduction Program (NHERP) provisions (BSSC 2015).

These experimentally inferred seismic design factors are also summarized in Fig. 18. Notably, the inferred overstrength factor Ω_o of ~3.4 is consistent with the design value ($\Omega_o = 3.0$). In contrast, the building response modification coefficient (R-factor) is determined to be ~3.6 from the test data, which is substantially smaller than the recommended value of 6.5. Because the R-factor

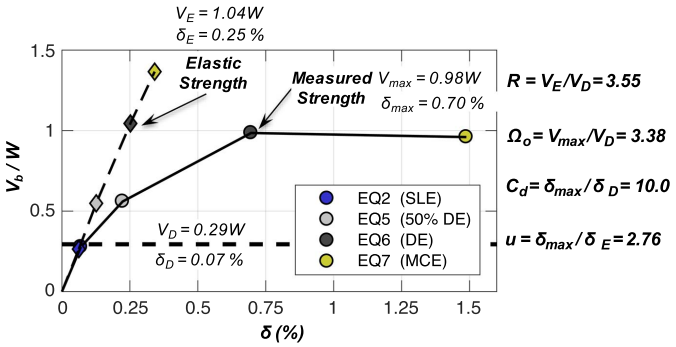

Fig. 18. Determination of key seismic design factors using measured peak roof drift ratio versus normalized base shear (V_b/W) responses (solid line) during the four select earthquake tests with the corresponding linear responses (dashed line).

is commonly considered as the product of the ductility reduction factor R_d and overstrength factor Ω_o (Uang 1991; Miranda and Bertero 1994), this implies that the test building may need to attain a greater ductility demand during the design event if an R-factor of 6.5 is considered in the seismic design. These results highlight the need for future system-level experiments to provide additional evidence for the R-factor assessment associated with the seismic design of CFS shear wall structures.

Conclusions

A unique full-scale midrise CFS-framed building is tested during a sequence of earthquake and live fire tests (Hutchinson et al. 2021). Importantly, these system-level building tests permit investigation of the component-level seismic behavior of CFS shear walls and their interactions under realistic earthquake loading environments and realistic boundary conditions. In this paper, the shear wall local responses measured during the earthquake tests are investigated and correlated with the building global responses in an effort to advance understanding of the seismic behavior of the shear walls and in particular the interactions among different shear walls (e.g., shear walls located along the same wall line or in the same quadrant). Additionally, important CFS seismic design parameters

are inferred from the measured building responses using a parameter optimization strategy. Findings regarding the seismic behavior of the shear walls and the seismic design of CFS shear wall structures include the following:

- The measured panel shear distortions of the corridor shear walls were consistently larger than those of the corner exterior shear walls at the same level. This may be attributed to the fact that the large aspect ratio (>4:1) of the corridor shear walls may lead to increased flexural deformation and reduced shear deformation during lateral loading. Further experimental studies may be conducted to understand the effect of aspect ratios on the shear wall local behavior. As a result of smaller panel shear distortion demands, the exterior shear walls sustained less severe seismic damage compared with the corridor shear walls at the same levels.
- Shear wall segments located at the same wall line and of similar length along the corridor of the building achieved comparable local responses (i.e., sheathing panel shear distortions, wall end vertical displacements, and tie-rod forces) during the earthquake tests. This indicates that individual corridor shear walls performed as individual wall segments, i.e., Type I systems, in response to lateral earthquake loads. In contrast, the measured local responses of the exterior shear walls located at the same wall line appeared less correlated. Instead, the tie-rod force distribution pattern implies that the exterior walls at the corners of the building interacted directly with the adjacent interior shear walls via the kinematic constraints of the floor diaphragm.
- An instance of tie-rod coupler connection failure was detected following the extreme event (final) test. Because the tensile forces of the disconnected tie rods were well below its (nominal) yield strength, the connection failure is more likely due to the extremely large story drift demands (>12%) imposed on the tie-down assembly. Nonetheless, this undesirable connection failure emphasizes the need for future studies to assess the behavior of the tie rods and their connections in response to extreme story drift demands.
- The building periods and damping ratios during the service-level earthquake tests indicate that the fundamental period of the building estimated in accordance with the ASCE-7 provisions (ASCE 2016) is ~30% larger than those identified from the test data. Additionally, the identified damping ratio of 8%–10% is 1.5–2.0 times that of the typical upper bound value of 5% recommended by the design guidelines (FEMA 2018). These observations are consistent with the findings from the shake-table experiments of a code-compliant CFS shear wall structure (Peterman et al. 2016a). It is therefore recommended that these observations be considered in future CFS building design applications.
- The experimentally inferred overstrength factor Ω_o of the test building (~3.4) is consistent with the design target value ($\Omega_o = 3.0$), however, the inferred response modification factor R appears substantially smaller than the code recommended value of 6.5. Because the R-factor is commonly considered as the product of the ductility reduction factor R_d and overstrength factor Ω_o, this implies that the test building may need to attain higher ductility demand during the design event if an R-factor of 6.5 is considered in seismic design. Further system-level experiments are strongly recommended to provide additional evidence for assessing this critical design parameter associated with CFS shear wall structures.

Data Availability Statement

Some or all data, models, or code that support the findings of this study are available from the corresponding author upon request.

Acknowledgments

This research project is a collaboration between two academic institutions (University of California, San Diego, and Worcester Polytechnic Institute), two government or institutional granting agencies (Department of Housing and Urban Development and the California Seismic Safety Commission) and more than 15 industry partners. The Jacobs School of Engineering and Department of Structural Engineering at UCSD also provided matching support for this effort. Although UCSD led the overall test program with their primary focus on the earthquake test phases, the authors are grateful to Professor Brian Meacham and Dr. Praveen Kamath (formerly with WPI) for their leading efforts on the fire testing and contribution to the overall test program. The active collaboration with Professor Gilbert Hegemier from UCSD in this test program is also greatly appreciated. Industry sponsors include the California Expanded Metal Products Co. (CEMCO) and Sure-Board, who each provided financial, construction, and materials support. Specific individuals that dedicated significant time on behalf of this effort included Fernando Sesma (CEMCO), Kelly Holcomb, Carleton Elliot, and Tyler Elliot (Sure-Board), Harry Jones (DCI Engineers), Diego Rivera (SWS Panels), Doug Antuma (Rivante), Larry Stevig (State Farm Insurance), Tim Reinhold and Warner Chang (Insurance Institute for Business and Home Safety), Steve Helland (DPR Construction), Rick Calhoun (Walters & Wolf), and Jesse Karnes (MiTek). The authors appreciate the efforts of these individuals and their colleagues at their respective firms. In addition, the NHERI@UCSD staff, namely, Robert Beckley, Jeremy Fitcher, Dan Radulescu, and Alex Sherman, as well as the UCSD graduate student Srikar Gunisetty, provided technical support for the test program. Their efforts are also greatly appreciated.

References

AISI (American Iron and Steel Institute). 2015a. *North American specification for the design of cold-formed steel structural framing*. AISI S240. Washington, DC: AISI.

AISI (American Iron and Steel Institute). 2015b. *North American standard for seismic design of cold-formed steel structural systems*. AISI S400. Washington, DC: AISI.

ASTM. 2018. *Standard specification for high-strength steel bars for prestressed concrete*. ASTM A722/A722M-18. West Conshohocken, PA: ASTM.

ASTM. 2019. *Standard specification for carbon structural steel*. ASTM A36/A36M-19. West Conshohocken, PA: ASTM.

ASTM. 2020. *Standard specification for alloy-steel and stainless steel bolting for high temperature or high pressure service and other special purpose applications*. ASTM A193/A193M-20. West Conshohocken, PA: ASTM.

Arias, A. 1970. "A measure of earthquake intensity." In *Seismic design for nuclear power plants*, edited by R. J. Hansen, 438–483. Cambridge, MA: MIT Press.

ASCE. 2016. *Minimum design loads for buildings and other structures*. ASCE 7. Reston, VA: ASCE.

Balh, N., J. DaBreo, C. Ong-Tone, K. El-Saloussy, C. Yu, and C. A. Rogers. 2014. "Design of steel sheathed cold-formed steel framed shear walls." *Thin-Walled Struct.* 75 (Feb): 76–86. https://doi.org/10.1016/j.tws.2013.10.023.

BSSC (Building Seismic Safety Council). 2015. *NEHRP recommended seismic provisions for new buildings and other structures, Volume 1: Part 1 provisions, part 2 commentary*. FEMA P-1050-1. Washington, DC: BSSC.

Cruz, C., and E. Miranda. 2016. "Evaluation of damping ratios for the seismic analysis of tall buildings." *ASCE J. Struct. Eng.* 143 (1): 04016144. https://doi.org/10.1061/(ASCE)ST.1943-541X.0001628.

Cruz, C., and E. Miranda. 2019. "Reliability of damping ratios inferred from the seismic response of buildings." *Eng. Struct.* 184 (Apr): 355–368. https://doi.org/10.1016/j.engstruct.2019.01.056.

FEMA (Federal Emergency Management Agency). 2018. *Guidelines for performance-based seismic design of buildings*. FEMA P-58-6. Washington, DC: FEMA.

Fiorino, L., B. Bucciero, and R. Landolfo. 2019. "Shake table tests of three storey cold-formed steel structures with strap-braced walls." *Bull. Earthquake Eng.* 17 (7): 4217–4245. https://doi.org/10.1007/s10518-019-00642-z.

Fiorino, L., V. Macillo, and R. Landolfo. 2017. "Shake table tests of a full-scale two-story sheathing-braced cold-formed steel building." *Eng. Struct.* 151 (Nov): 633–647. https://doi.org/10.1016/j.engstruct.2017.08.056.

Fülöp, L., and D. Dubina. 2004. "Performance of wall-stud cold-formed shear panels under monotonic and cyclic loading: Part I: Experimental research." *Thin-Walled Struct.* 42 (2): 321–338. https://doi.org/10.1016/S0263-8231(03)00063-6.

Hutchinson, T. C., X. Wang, G. Hegemier, P. Kamash, and B. Meacham. 2021. "Earthquake and post-earthquake fire testing of a mid-rise cold-formed steel framed building. I: Building response and physical damage." *J. Struct. Eng.* 147 (9): 04021125. https://doi.org/10.1061/(ASCE)ST.1943-541X.0003097.

Iuorio, O., V. Macillo, M. T. Terracciano, T. Pali, L. Fiorino, and R. Landolfo. 2014. "Seismic response of CFS strap-braced stud walls: Experimental investigation." *Thin-Walled Struct.* 85 (Dec): 466–480. https://doi.org/10.1016/j.tws.2014.09.008.

Kramer, S. L. 1996. *Geotechnical earthquake engineering*. Upper Saddle River, NJ: Prentice-Hall.

Liu, P., K. D. Peterman, and B. W. Schafer. 2014. "Impact of construction details on OSB-sheathed cold-formed steel framed shear walls." *J. Constr. Steel Res.* 101 (Oct): 114–123. https://doi.org/10.1016/j.jcsr.2014.05.003.

Miranda, E., and V. V. Bertero. 1994. "Evaluation of strength reduction factors for earthquake-resistant design." *Earthquake Spectra* 10 (2): 357–379. https://doi.org/10.1193/1.1585778.

Peterman, K. D., M. J. Stehman, R. L. Madsen, S. G. Buonopane, N. Nakata, and B. W. Schafer. 2016a. "Experimental seismic response of a full-scale cold-formed steel-framed building. I: System-level response." *ASCE J. Struct. Eng.* 142 (12): 04016127. https://doi.org/10.1061/(ASCE)ST.1943-541X.0001577.

Peterman, K. D., M. J. Stehman, R. L. Madsen, S. G. Buonopane, N. Nakata, and B. W. Schafer. 2016b. "Experimental seismic response of a full-scale cold-formed steel-framed building. II: Subsystem-level response." *J. Struct. Eng.* 142 (12): 04016128. https://doi.org/10.1061/(ASCE)ST.1943-541X.0001578.

Serrette, R., J. Encalada, M. Juadines, and H. Nguyen. 1997. "Static racking behavior of plywood, OSB, gypsum, and fiberboard walls with metal framing." *ASCE J. Struct. Eng.* 123 (8): 1079–1086. https://doi.org/10.1061/(ASCE)0733-9445(1997)123:8(1079).

Uang, C. M. 1991. "Establishing R (or Rw) and Cd factors for building seismic provisions." *J. Struct. Eng.* 117 (1): 19–28. https://doi.org/10.1061/(ASCE)0733-9445(1991)117:1(19).

Van Overschee, P., and B. De Moor. 1996. *Subspace system identification for linear systems*. Boston: Kluwer.

Wang, X., and T. C. Hutchinson. 2020. "Evolution of modal characteristics of a mid-rise cold-formed steel building during construction and earthquake testing." *Earthquake Eng. Struct. Dyn.* 49 (14): 1539–1558. https://doi.org/10.1002/eqe.3316.

Wang, X., T. C. Hutchinson, G. Hegemeir, S. Gunisetty, P. Kamath, and B. Meacham. 2016. *Earthquake and post-earthquake fire performance of a mid-rise cold-formed steel framed building—Test program and test results: Final Report (CFS Test Program Report #2). Structural Systems Research Project*. Rep. No. SSRP-16/08. La Jolla, CA: Univ. of California, San Diego.

Yu, C. 2010. "Shear resistance of cold-formed steel framed shear walls with 0.686 mm, 0.762 mm, and 0.838 mm steel sheet sheathing." *Eng. Struct.* 32 (6): 1522–1529. https://doi.org/10.1016/j.engstruct.2010.01.029.

Zhang, W., M. Mahdavian, Y. Li, and C. Yu. 2016. "Experiments and simulations of cold-formed steel wall assemblies using corrugated steel sheathing subjected to shear and gravity loads." *ASCE J. Struct. Eng.* 143 (4): 04016193. https://doi.org/10.1061/(ASCE)ST.1943-541X.0001681.

Zhang, W., M. Mahdavian, Y. Li, and C. Yu. 2017. "Seismic performance evaluation of cold-formed steel shear walls using corrugated steel sheathing." *ASCE J. Struct. Eng.* 143 (11): 04017151. https://doi.org/10.1061/(ASCE)ST.1943-541X.0001891.